

Radiological environmental impact analysis of a 2-MW thorium molten salt reactor during an accident

Chang-Qi Chen^{1,2} · Xiao-Bin Xia¹ · Zhi-Hong Zhang¹ · Jun Cai¹ · Chang-Yuan Li¹

Received: 9 July 2018 / Revised: 29 October 2018 / Accepted: 19 November 2018 / Published online: 11 April 2019
© China Science Publishing & Media Ltd. (Science Press), Shanghai Institute of Applied Physics, the Chinese Academy of Sciences, Chinese Nuclear Society and Springer Nature Singapore Pte Ltd. 2019

Abstract The thorium molten salt reactor–liquid fuel (TMSR-LF1) has inherent safety features. The accident occurrence possibility and their consequences are much lower for the TMSR-LF1 than that of traditional reactors. Based on accident analysis, the maximum credible accident and the radioactive source terms of the TMSR-LF1 were first estimated. Then, the total effective dose of the maximum credible accident was calculated. Based on calculations, the cover gas flow rate can significantly affect the radiation consequences of the maximum credible accident when it changes from 0 to 10 L/min. If no cover gas is flowing, a site-area emergency would be required within the range of 50–73 m from the reactor. In the case of cover gas flow, only an abnormal notification and an alert two emergency class would be required within the range of 50 m.

Keywords TMSR-LF1 · Accident classification and description · Maximum credible accident · Emergency class

1 Introduction

The molten salt reactor (MSR) is among the six advanced reactor types proposed in the Generation IV International Forum [1]. The Chinese Academy of Sciences launched a thorium molten salt reactor–liquid fuel (TMSR-LF1), a type of MSR, to develop the fourth-generation advanced nuclear energy technology [2–5]. From a safety perspective, the TMSR-LF1 has several characteristics: a negative feedback mechanism, no risk of fuel melt, low-pressure operation, cooling without water, an online cover gas purge system, and a redundant passive air-cooled system [6–9].

The accident occurrence possibility and their consequences are much lower for the TMSR-LF1 than that of traditional reactors. For increased safety, a systematic and complete radiological environmental impact should be analyzed to support nuclear emergency preparedness and response for reactors.

A number of mature studies of radiological environmental impact have been conducted on nuclear power plants [10–13]. Studies of the radiological environmental impact of research reactors are fewer than those of nuclear power plants because of the complex reactor types. Sutton's formula was used in radiological environmental impact analysis for the Molten Salt Reactor Experiment (MSRE) [14]. As time has passed, Sutton's formula has rarely been used in radiological environmental impact analysis. A systematic restudy of the radiological environmental impact of MSRs is necessary.

This study attempted to determine the maximum credible accident and its consequence among all possible nuclear accidents of the TMSR-LF1, assess the radioactive severity of the consequences of the maximum credible

✉ Xiao-Bin Xia
xiaxiaobin@sinap.ac.cn

¹ Shanghai Institute of Applied Physics, Chinese Academy of Sciences, Shanghai 201800, China

² University of Chinese Academy of Sciences, Beijing 100049, China

accident, and discuss the corresponding emergency preparedness for the TMSR-LF1.

2 Inventory of radionuclides in the TMSR-LF1

2.1 Radionuclides produced in core

Radioactive materials in the fuel molten salt of the TMSR-LF1 mainly originate from three sources as follows:

- 1) Fission products from the core fuel.
- 2) Neutron activation products from the molten salt and impurities in it.
- 3) Neutron activation of corrosion products from pipe and heat exchanger structural materials.

The TMSR-LF1 parameters are shown in Table 1. Considering the aforementioned three sources and cover gas purges, the inventory of radionuclides in the core fuel of the TMSR-LF1 after 60 days continuing full power operation can be calculated using SCALE6.1 [15] as shown in Table 2.

2.2 Inventory of radionuclides in cover gas

Experimental data on the MSRE show that, under normal conditions, most of the noble gases via fission in the molten salt would diffuse into the cover gas. A small amount (less than 1%) of iodine would diffuse into the cover gas from the fuel molten salt [16]. In addition, approximately 50% of the tritium would diffuse into the cover gas [17].

Figure 1 shows the major radionuclide migration path in the TMSR-LF1. Under the normal operational condition of the TMSR-LF1, fuel mainly originates from fission and

neutron activation products. All the noble gas and a portion of the iodine produced by the fission reaction would diffuse from the fuel salt into the cover gas system. The TMSR-LF1 uses argon gas as a cover gas. The cover gas also can be neutron activated. During reactor operation, cover gas would flow through the fuel salt into the exhaust system. Finally, the treated radioactive gas is discharged into the environment through the chimney.

According to the design of the TMSR-LF1, the cover gas flows at a constant rate. It is assumed that 100% of the noble gas and 10% of the iodine would enter the cover gas from the fuel salt. In addition, among all the neutron activation products listed in Table 2, only ^{14}C and tritium would release from the molten salt into the cover gas. Conserve assume that all ^{14}C would enter the cover gas in the form of CO_2 .

Tritium release should be a concern as a large amount of tritium is generated through the neutron adsorption of lithium [18]. Tritium is absorbed and desorbed by graphite and permeates through structural materials [19]. In the TMSR-LF1, most tritium permeates through the metal walls to the surroundings at high temperatures [20]. Except for the part absorbed by graphite, tritium does not concentrate somewhere in the reactor for very long. Approximately 91.76% of the tritium continuously permeates out to the environment during the whole operational period via the TMSR-TTAC [21] code. Therefore, radiological environmental impact of tritium would be assessed under normal operation and is beyond the scope of this article.

Radioactive materials pass from the molten salt fuel to the cover gas and decrease with the cover gas flowing. The atomic concentration $C_i(t)$ (atomic number/L) of a nuclide i in the cover gas is as follows:

$$\frac{dC_i(t)}{dt} = \frac{q_i}{V} - \frac{g}{V} C_i(t) - \lambda_i C_i(t), \quad (1)$$

where q_i (atomic number/s) is the average rate of nuclide i passing from the fuel salt into the cover gas; V (L) is the volume of the cover gas; λ_i (s^{-1}) is the decay constant of the nuclide i ; and g (L/s) is the cover gas flow rate.

The equation can be solved as follows:

$$C_i(t) = \frac{q_i}{g + \lambda_i V} \left(1 - e^{-(\lambda_i + \frac{g}{V})t} \right). \quad (2)$$

The equilibrium concentration of radionuclide i in the cover gas is as follows:

$$C_i(t) = \frac{q_i}{g + \lambda_i V}. \quad (3)$$

The time the nuclides pass from the fuel salt into the cover gas and the deposition of their decay daughters in the gas pipeline are ignored in the calculation.

The cumulative number of radioactive materials in the cover gas is related to the cover gas flow rate. Assuming

Table 1 TMSR-LF1 parameters

Parameters	Value
Thermal power (MW)	2
Lifetime (years)	10
Effective full power days (days/year)	60
Fuel composition	LiF-BeF ₂ -ZrF ₄ -UF ₄
Fuel salt load (m ³)	1.68
⁷ Li abundance (at.%)	> 99.95
²³⁵ U enrichment (wt%)	19.75
Fuel inlet temperature (°C)	630
Fuel outlet temperature (°C)	650
Volume	
Fuel salt volume (m ³)	1.68
Cover gas volume (m ³)	1.6

Table 2 Inventory of radionuclides in the fuel salt of TMSR-LF1 after 60 days of full power operation (Bq)

Nuclide	Activity	Nuclide	Activity	Nuclide	Activity	Nuclide	Activity
Fission products							
⁸⁸ Rb	2.21×10^{15}	¹⁰⁶ Rh	2.88×10^{13}	¹³² I	2.44×10^{15}	¹⁴² La	3.67×10^{15}
⁸⁹ Sr	1.67×10^{15}	¹⁰⁶ Ru	2.71×10^{13}	¹³² Te	2.70×10^{15}	¹⁴³ Pr	3.42×10^{15}
⁹⁰ Sr	1.43×10^{13}	^{110m} Ag	1.14×10^8	¹³³ I	3.79×10^{15}	¹⁴⁴ Ce	4.69×10^{14}
⁹⁰ Y	1.36×10^{13}	^{115m} Cd	2.58×10^{11}	¹³³ Te	2.33×10^{15}	¹⁴⁴ Pr	4.69×10^{14}
⁹¹ Sr	3.64×10^{15}	¹²³ Sn	1.81×10^{11}	¹³⁴ Cs	3.92×10^{10}	¹⁴⁷ Nd	1.38×10^{15}
⁹¹ Y	1.84×10^{15}	¹²⁵ Sb	8.12×10^{11}	¹³⁴ I	4.42×10^{15}	¹⁴⁷ Pm	4.46×10^{13}
⁹² Sr	3.73×10^{15}	¹²⁵ Sn	6.20×10^{12}	¹³⁵ I	3.55×10^{15}	¹⁴⁸ Pm	1.17×10^{12}
⁹⁵ Nb	8.86×10^{14}	^{125m} Te	5.26×10^{10}	¹³⁶ Cs	2.80×10^{12}	^{148m} Pm	3.71×10^{11}
^{95m} Nb	1.99×10^{13}	¹²⁷ Sb	9.88×10^{13}	^{137m} Ba	1.39×10^{13}	¹⁵¹ Sm	3.19×10^{11}
⁹⁵ Zr	1.97×10^{15}	¹²⁷ Sn	6.01×10^{13}	¹³⁷ Cs	1.45×10^{13}	¹⁵⁴ Eu	1.40×10^9
⁹⁷ Zr	3.83×10^{15}	¹²⁷ Te	8.78×10^{13}	¹³⁸ Cs	4.22×10^{15}	¹⁵⁵ Eu	4.65×10^{11}
⁹⁹ Mo	3.85×10^{15}	¹²⁹ Te	3.13×10^{14}	¹³⁹ Ba	4.02×10^{15}	¹⁵⁶ Eu	9.63×10^{12}
^{99m} Te	3.39×10^{15}	^{129m} Te	4.05×10^{13}	¹⁴⁰ Ba	3.75×10^{15}	¹⁶⁰ Tb	8.60×10^7
^{103m} Rh	1.23×10^{15}	¹³¹ I	1.60×10^{15}	¹⁴⁰ La	3.73×10^{15}	²³⁹ Am	1.75×10^{-3}
¹⁰³ Ru	1.25×10^{15}	¹³¹ Te	1.63×10^{15}	¹⁴¹ Ce	2.64×10^{15}	²⁴⁰ Am	3.06×10^{-1}
²⁴² Am	1.20×10^6	^{131m} Te	2.47×10^{14}	¹⁴¹ La	3.67×10^{15}	²⁴¹ Am	4.48×10^4
^{242m} Am	2.23×10^1	²⁴³ Cm	9.41×10^0	²³⁹ Pu	5.01×10^{10}	²³³ U	1.76×10^2
²⁴³ Am	3.07×10^{-1}	²⁴⁴ Cm	1.52×10^1	²⁴⁰ Pu	5.07×10^8	²³⁴ U	1.70×10^5
²⁴⁴ Am	2.48×10^0	²⁴⁵ Cm	1.83×10^{-5}	²⁴¹ Pu	7.08×10^8	²³⁵ U	3.78×10^9
^{244m} Am	3.89×10^1	²⁴⁶ Cm	1.86×10^{-8}	²⁴² Pu	2.17×10^1	²³⁶ U	6.53×10^7
²⁴⁵ Am	3.96×10^{-7}	²³⁷ Np	2.11×10^5	²⁴³ Pu	9.16×10^4	²³⁷ U	6.34×10^{12}
²⁴¹ Cm	1.09×10^{-5}	²³⁹ Np	1.11×10^{16}	²³² U	1.18×10^4	²³⁸ U	2.51×10^9
²⁴² Cm	4.67×10^4	²³⁶ Pu	6.57×10^1	²⁴⁰ Pu	5.07×10^8	²³⁹ U	1.12×10^{16}
^{83m} Kr	3.38×10^{14}	²³⁸ Pu	3.47×10^6	¹³⁵ Xe	3.69×10^{15}	¹³³ I	4.21×10^{15}
⁸⁵ Kr	1.97×10^{12}	⁸⁸ Kr	2.19×10^{15}	^{135m} Xe	7.63×10^{14}	¹³⁴ I	4.91×10^{15}
^{85m} Kr	7.98×10^{14}	^{131m} Xe	1.80×10^{13}	¹³¹ I	1.78×10^{15}	¹³⁵ I	3.94×10^{15}
⁸⁷ Kr	1.63×10^{15}	¹³³ Xe	3.99×10^{15}	¹³² I	2.71×10^{15}	^{133m} Xe	1.11×10^{14}
Neutron activation of corrosion products							
⁵¹ Cr	2.27×10^{12}	⁵⁸ Co	1.89×10^{10}	⁵⁴ Mn	1.60×10^9	⁶⁵ Ni	7.81×10^9
⁵⁶ Mn	4.38×10^{12}	⁵⁵ Fe	3.84×10^{10}	⁵⁹ Ni	1.36×10^7		
⁶⁰ Co	1.42×10^{11}	⁵⁹ Fe	1.61×10^7	⁶³ Ni	1.66×10^9		
Neutron activation of impurities							
⁸ Li	1.29×10^{15}	¹⁶ N	5.28×10^{14}	³ H	1.57×10^{14}	²⁰ F	9.31×10^{14}
⁶ He	3.23×10^{14}	¹⁹ O	3.69×10^{13}	¹⁴ C	6.14×10^8		

that the cover gas flow rate is 4 L/min, 10 L/min, 50 L/min, 100 L/min, and 0 L/min, respectively, the inventory of radionuclides in the cover gas of the TMSR-LF1 after 60 days continuing full power operation was calculated and is shown in Table 3.

3 Accident classification and description of the TMSR-LF1

The main reactor structures of the TMSR-LF1 are shown in Fig. 2. All the fuel salt is contained in the reactor vessel. Outside of the reactor vessel are a safety vessel and

concrete containment. The cavity is divided into an upper and lower cavity. The entire cavity is belowground, and the reactor vessel is in the lower cavity.

3.1 Accident classification of the TMSR-LF1

All possible TMSR-LF1 accidents are listed in Table 4. According to the previous analysis in chapter 2, TMSR-LF1 radioactivity is concentrated in the fuel salt and cover gas. Thus, the integrity of the fuel and cover gas boundaries determines the possibility of a radioactive release occurring. From this perspective, fuel salt and cover gas leaks undoubtedly need attention. In addition, unexpected

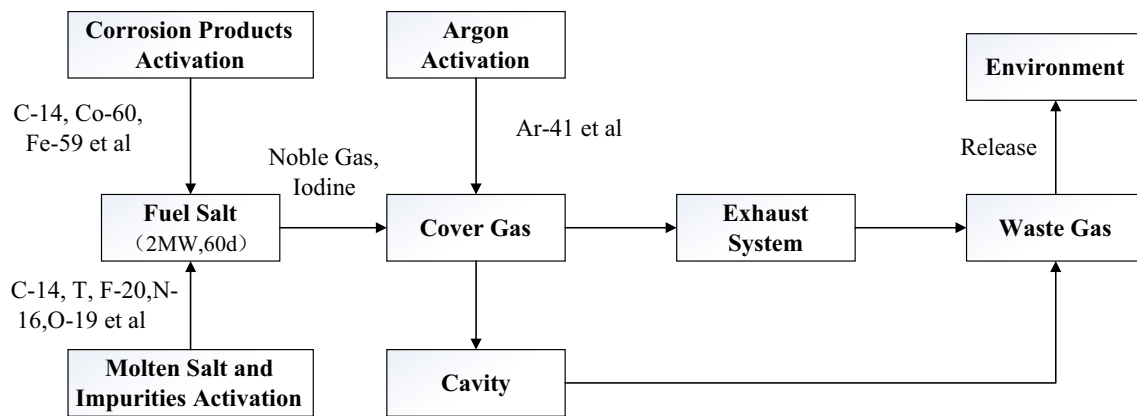


Fig. 1 Major radionuclide migration path in the TMSR-LF1

Table 3 Inventory of radionuclides in the cover gas of the TMSR-LF1 after 60 days of full power operation (Bq)

Nuclide	Flow rate (L/min)				
	0	4	10	50	100
^{14}C	6.14×10^8	2.72×10^5	1.09×10^5	2.18×10^4	1.09×10^4
^{37}Ar	1.15×10^{10}	9.08×10^7	3.65×10^7	7.30×10^6	3.65×10^6
^{39}Ar	2.62×10^5	1.22×10^3	4.87×10^2	9.74×10^1	4.87×10^1
^{41}Ar	6.62×10^{11}	4.75×10^{11}	3.33×10^{11}	1.11×10^{11}	6.08×10^{10}
$^{83\text{m}}\text{Kr}$	2.00×10^8	1.43×10^8	9.98×10^7	3.32×10^7	1.81×10^7
^{85}Kr	1.89×10^{11}	8.75×10^8	3.50×10^8	7.00×10^7	3.50×10^7
$^{85\text{m}}\text{Kr}$	5.36×10^{11}	2.72×10^{11}	1.57×10^{11}	4.09×10^{10}	2.12×10^{10}
^{87}Kr	3.98×10^{13}	3.13×10^{13}	2.36×10^{13}	8.98×10^{12}	5.06×10^{12}
^{88}Kr	1.49×10^{14}	9.29×10^{13}	5.93×10^{13}	1.74×10^{13}	9.24×10^{12}
$^{131\text{m}}\text{Xe}$	3.44×10^8	3.28×10^5	1.00×10^5	1.66×10^4	8.06×10^3
^{133}Xe	7.74×10^{11}	6.52×10^9	1.64×10^9	2.00×10^8	9.10×10^7
$^{133\text{m}}\text{Xe}$	1.81×10^{11}	1.32×10^{10}	5.48×10^9	1.12×10^9	5.59×10^8
^{135}Xe	2.78×10^{13}	5.13×10^{12}	1.88×10^{12}	3.00×10^{11}	1.42×10^{11}
$^{135\text{m}}\text{Xe}$	1.92×10^{13}	1.58×10^{13}	1.40×10^{13}	8.94×10^{12}	6.28×10^{12}
^{131}I	3.33×10^{10}	7.84×10^8	3.18×10^8	6.41×10^7	3.21×10^7
^{132}I	7.79×10^{10}	5.22×10^{10}	3.49×10^{10}	1.09×10^{10}	5.85×10^9
^{133}I	7.39×10^{11}	1.33×10^{11}	5.98×10^{10}	1.28×10^{10}	6.45×10^9
^{134}I	4.29×10^{12}	3.59×10^{12}	2.89×10^{12}	1.26×10^{12}	7.39×10^{11}
^{135}I	2.54×10^{13}	1.04×10^{13}	5.51×10^{12}	1.33×10^{12}	6.84×10^{11}

reactivity initiation and a decrease in the core heat removal are both suspected to overheat the reactor core and may damage the core boundary. The four accident types are described in detail in the next section. As for unexpected natural disasters such as earthquakes, the possibility of occurrence is too low to be considered in this study.

3.2 Reactivity initiated accident and core heat removal decrease accident

A reactivity initiated accident is an important part of reactor safety analysis because the consequence of initiating reactivity transient affects reactor safety. The reactivity

coefficients of the TMSR-LF1, such as the fuel temperature reactivity, reactivity power, and graphite reactivity temperature coefficients, are negative [9, 23]. The negative feedback mechanism enables the TMSR-LF1 to maintain a steady state. During all the transient conditions, the maximum temperature of the fuel salt and graphite is far below the temperature limit of the material. Therefore, a reactivity initiated accident would not damage the core boundary and release radioactivity.

An extended and verified RELAP5 code was used to perform transient safety analysis for the TMSR-LF1 [8]. The results show that the temperature of the TMSR-LF1 would not exceed the safety limits given a decrease in core

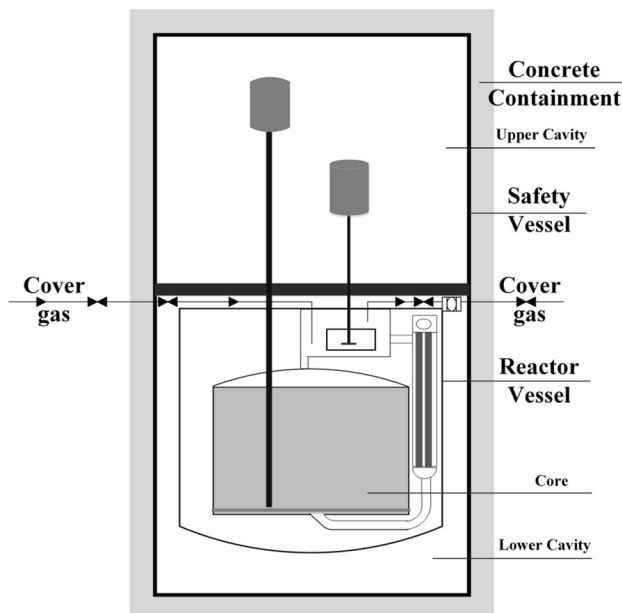


Fig. 2 Schematic of main reactor structures in the TMSR-LF1

heat removal. For example, when a station blackout accident occurred, the increased core temperature would be 4 °C. Therefore, core heat removal decrease accident would not damage the core boundary and release radioactivity.

3.3 Fuel salt leak

In the MSRE, it is considered credible that a rupture of pipelines and facilities can lead to a release of molten salt fuel from the fuel circulation system into the reactor containment. Based on the safety analysis of the MSREMSRE, its maximum credible accident is a simultaneous molten salt and water leak. High-temperature molten salt and water would form mixed steam and maximize the secondary container pressure. No more than 4 L of molten salt would finally leak during the maximum credible accident

[14]. After molten salt fuel leakage from the fuel circle system, most would be contained in containment. Only gaseous nuclides can pass through containment and release into the building, including 100% of the noble gas, 10% of the iodine with a 50% plate out on the secondary container surfaces, and 10% of the fissile metals will disperse from the molten salt into the air. The radioactive release from the container to the building would take 4 h [14].

Assume the fuel molten salt would leak from a rupture of equipment or weld seams and the maximum leakage of the fuel salt is 4 L. There is no water in the TMSR-LF1 so a mixed steam of molten salt and water would not appear following a fuel salt leak. Therefore, only a molten salt leak would not result in too much pressure on the reactor or safety vessels [14].

Because of the influence of gravitational potential energy, molten salt running from the fuel cycle will flow downward after the accident occurs. Except for extreme cases such as earthquakes, run-off molten salt can hardly erupt upward. The run-off molten salt would remain in the reactor vessel with high probability, not affecting the safety vessel and outside environment. In consideration that there is no historical record of destructive earthquakes at the plant site of the TMSR-LF1 and surrounding area, particularly no digital record from instruments after 1970, this study did not consider the occurrence of earthquakes [24].

Another scenario is that leaking molten salt has the rare chance to break through the physical barrier of the reactor vessel into the lower cavity. The melting point of the fuel salt of the TMSR-LF1 is approximately 450 °C, and the lower cavity temperature is lower than this melting point; leaking molten salt would coagulate as the temperature decreases. The heat dissipating capacity of the cavity is 40 Kw [24], assuming that 90% of the heat dissipating capacity is used in core residual heat discharge and 10% is used to discharge heat from the leaking molten salt. The leaking fuel salt would coagulate from 650 to 450 °C in approximately 15 min. Radioactive nuclides stored in the

Table 4 Accident classification and initiating conditions of the TMSR-LF1 [22]

Accident classification	Initiating condition
Reactivity initiated accident	An uncontrolled rod withdrawal under subcriticality or low power, an uncontrolled rod withdrawal under power operation, accidental criticality during the process of charging
Core heat removal decrease accident	Molten salt pump rotor seizure accident, station blackout, loss of heat sink, air cooling fan failure
Core heat removal increase accident	Increase in cooling salt flow, decrease in cooling salt temperature
Facility leakage	Fuel salt leak, cover gas leak
Anticipated transient without scram (ATWS)	Loss of outer power without scram, uncontrolled rod withdrawal without scram
Hazards and other conditions affecting reactor	Earthquake, flooding, explosion, fire

run-off fuel salt would have difficulty releasing in 15 min as well as residual fission products and decay products. Outside of the lower cavity are a safety vessel and concrete containment to stop radioactive materials. Therefore, a fuel salt leak accident can hardly result in a radiation impact on the building and external environment.

3.4 Cover gas leak

In the TMSR-LF1, an online cover gas purge system can remove radioactive nuclides from the molten salt fuel to the cover gas during reactor operation. A mass cumulated number of radioactive nuclides may exist in the cover gas. Thus, the complete release of radioactive materials in the cover gas should be carefully considered and analyzed [10, 22].

Suppose all the cover gas leaks from a rupture of equipment or weld seams into the safety vessel at maximum fuel burnup. When the low-pressure signal of the cover gas system reaches the reactor trip set points, reactor control rods will fall for scram in 30 s (or be manually shutdown by operators according to the monitoring display). At the same time, the residual heat removal system starts and the residual heat of the core will be derived.

During this accident, new radioactivity would be produced during the 30 s scram process and then enter in the cover gas from the molten salt in the same ratio as that mentioned in Sect. 2.2. These radionuclides passing into the cover gas are listed in Table 5.

All the radioactive materials stored in the cover gas system and those produced during the scrambling process are first released into the safety vessel. The leakage rate of the safety vessel to the building hall is 5 vol%/d; all the gaseous radioactive materials will release into building following the accident within 24 h. Because the number of radioactive materials in cover gas is related to the gas flow rate, the source terms of the cover gas leak accident are also closely related to the flow rate. In addition, as xenon could be produced by the decay of iodine, radioactive decay was considered in the calculation. The source terms of the cover gas leak releasing into the building at each flow rate are listed in Table 6. The main source terms are krypton, xenon, and iodine.

4 Maximum credible accident

According to the aforementioned accident analysis of the TMSR-LF1, among all the possible accident types, only the cover gas leak may lead to serious radioactive release. Therefore, the cover gas leak was chosen as the maximum credible accident.

The 24-h cumulative dose at the site boundary of an individual without any protection measures after an accident occurs should be considered when developing an emergency plan for a research reactor [25]. The 24-h total effective dose is considered as a sum of the external exposure from plume immersion and internal exposure from inhalation. Calculated formulas are as follows [26]:

$$H_p = \sum_i C_i \cdot (\chi/Q) \cdot t \cdot DCF_{p,i} \cdot S_p, \quad (4)$$

$$H_b = \sum_i C_i \cdot (\chi/Q) \cdot t \cdot DCF_{b,i} \cdot B \cdot S_b, \quad (5)$$

where H (Sv) is the cumulative radiation dose; C_i (Bq) is the release concentration of a nuclide i ; χ/Q ($s \cdot m^{-3}$) is the atmospheric diffusion factor; t (s) is the diffusion time; $DCF_{p,i}$ ($Sv \cdot (Bq \cdot s \cdot m^{-3})^{-1}$) is the dose coefficient for air submersion; $DCF_{b,i}$ ($Sv \cdot Bq^{-1}$) is the dose coefficient for inhalation; B ($m^3 \cdot s^{-1}$) is the respiration rate; and S (l) is the shielding factor.

The aforementioned dose coefficients of each radionuclide for two exposure paths that are used in calculation were taken from standards and guidance [27–29]. Adult respiratory rates were derived from Regulatory Guide 1.195 from the USA [30].

The ARCON96 code was chosen to calculate atmospheric diffusion factors [31, 32]. The ARCON96 code implements a straight-line Gaussian model with building wake and low wind speed corrections. These two corrections can effectively correct the dispersion consequence of the Gaussian model in power plant area [31, 33].

In the site plan, the distance from the reactor to the nearest site boundary is 73 m and the farthest distance is 942 m; thus, the calculation range was from 50 to 1000 m. Some site limit atmosphere diffusion factors are shown in Table 7 using meteorological data of the plan site.

Table 5 Radioactivity produced during 30-s scram process (Bq)

Nuclide	Activity	Nuclide	Activity	Nuclide	Activity
^{83m}Kr	5.90×10^7	^{131m}Xe	4.44×10^3	^{131}I	8.77×10^6
^{85}Kr	1.02×10^6	^{133}Xe	1.98×10^7	^{132}I	1.45×10^9
^{85m}Kr	2.47×10^{10}	^{133m}Xe	1.30×10^8	^{133}I	2.76×10^9
^{87}Kr	2.27×10^{12}	^{135}Xe	3.26×10^{10}	^{134}I	2.25×10^{11}
^{88}Kr	3.25×10^{12}	^{135m}Xe	2.51×10^{12}	^{135}I	2.34×10^{11}

Table 6 Source terms of the cover gas leak of the TMSR-LF1

Nuclide	Flow rate (L/min)				
	0	4	10	50	100
^{14}C	3.07×10^7	1.32×10^4	5.44×10^3	1.09×10^3	5.44×10^2
^{37}Ar	5.72×10^8	4.52×10^6	1.82×10^6	3.64×10^5	1.82×10^5
^{39}Ar	1.31×10^4	6.11×10^1	2.43×10^1	4.88×10^0	2.43×10^0
^{41}Ar	7.71×10^9	5.53×10^9	3.88×10^9	1.30×10^9	7.07×10^8
$^{83\text{m}}\text{Kr}$	2.75×10^6	2.07×10^6	1.57×10^6	7.85×10^5	6.06×10^5
^{85}Kr	9.45×10^9	4.38×10^7	1.75×10^7	3.55×10^6	1.80×10^6
$^{85\text{m}}\text{Kr}$	1.26×10^{10}	6.60×10^9	3.94×10^9	1.29×10^9	8.32×10^8
^{87}Kr	3.95×10^{11}	3.18×10^{11}	2.52×10^{11}	1.23×10^{11}	8.86×10^{10}
^{88}Kr	2.48×10^{12}	1.55×10^{12}	1.00×10^{12}	3.17×10^{11}	1.83×10^{11}
$^{131\text{m}}\text{Xe}$	1.72×10^7	2.23×10^4	7.55×10^3	1.51×10^3	8.46×10^2
^{133}Xe	3.87×10^{10}	4.96×10^8	1.61×10^8	2.77×10^7	1.39×10^7
$^{133\text{m}}\text{Xe}$	8.47×10^9	6.24×10^8	2.63×10^8	5.80×10^7	3.18×10^7
^{135}Xe	1.18×10^{12}	2.70×10^{11}	1.16×10^{11}	2.34×10^{10}	1.21×10^{10}
$^{135\text{m}}\text{Xe}$	1.50×10^{11}	1.17×10^{11}	8.81×10^{10}	4.91×10^{10}	3.51×10^{10}
^{131}I	1.63×10^9	3.88×10^7	1.60×10^7	3.54×10^6	1.97×10^6
^{132}I	1.13×10^9	7.38×10^8	4.97×10^8	1.63×10^8	9.32×10^7
^{133}I	3.07×10^{10}	5.60×10^9	2.57×10^9	6.23×10^8	3.60×10^8
^{134}I	2.98×10^{10}	2.55×10^{10}	2.07×10^{10}	9.48×10^9	5.92×10^9
^{135}I	7.35×10^{11}	3.05×10^{11}	1.63×10^{11}	4.28×10^{10}	2.42×10^{10}
Total	5.08×10^{12}	2.61×10^{12}	1.65×10^{12}	5.68×10^{11}	3.51×10^{11}

Calculation doses at the nearest site boundary ($d = 73$ m) for each cover gas flow rate are shown in Table 8.

From Table 8, the plume immersion exposure is the most influential exposure path. Its proportion is greater than 70%. The second highest proportion is inhalation exposure at greater than 20%.

Some concerning calculation doses in Table 8 are shown during different time periods in Table 9. The statistics of effective doses produced during three time periods following the maximum credible accident show their contributions to the 24-h total effective dose are approximately 29%, 51% and 19%, respectively. As a

simple average, the suffered dose per hour from 0 to 2 h phase accounted for 14.5% of the 24-h cumulative dose, the suffered dose per hour from 2 to 8 h phase accounted for 8.5%, and the suffered dose per hour from 8 to 24 h phase accounted for approximately 1.2%.

5 Discussion

5.1 Influence of the cover gas flow rate

Different cover gas flow rates would lead to different source terms for the maximum credible accident and then produce an effect on the maximum credible accident consequence; thus, the influence of cover gas flow rate is worth discussing. Figure 3a shows the proportions of some radionuclide inventories in the cover gas at each flow rate.

Table 7 Atmospheric diffusion factors of the plan site (s m^{-3})

Distance (m)	0–2 h	2–8 h	8–24 h
50	1.31×10^{-2}	1.11×10^{-2}	5.48×10^{-3}
73	5.93×10^{-3}	5.20×10^{-3}	2.55×10^{-3}
100	3.54×10^{-3}	2.96×10^{-3}	1.48×10^{-3}
150	2.28×10^{-3}	1.95×10^{-3}	9.66×10^{-4}
200	1.10×10^{-3}	9.66×10^{-4}	4.78×10^{-4}
250	6.27×10^{-4}	5.27×10^{-4}	2.65×10^{-4}
300	2.96×10^{-4}	2.48×10^{-4}	1.25×10^{-4}
400	1.75×10^{-4}	1.49×10^{-4}	7.47×10^{-5}
500	1.20×10^{-4}	9.97×10^{-5}	5.05×10^{-5}
1000	8.78×10^{-5}	7.39×10^{-5}	3.73×10^{-5}

Table 8 24-h total effective dose of the maximum credible accident at the nearest site boundary (mSv)

Flow rate (L/min)	Immersion	Inhalation	Total
0	1.53	0.958	2.49
4	0.910	0.361	1.27
10	0.590	0.194	0.78
50	0.197	0.052	0.250
100	0.119	0.030	0.149

Table 9 Effective dose of the maximum credible accident at the nearest site boundary ($d = 73$ m) for different times (mSv)

Flow rate (L/min)	0–2 h	2–8 h	8–24 h	0–24 h
0	0.731	1.28	0.475	2.49
4	0.399	0.65	0.218	1.27
10	0.255	0.401	0.128	0.78
50	8.67×10^{-2}	1.27×10^{-1}	3.60×10^{-2}	0.250
100	5.29×10^{-2}	7.65×10^{-2}	1.98×10^{-2}	0.149

Whether conducting cover gas flow purging or not has an obvious influence on the proportions of Kr and Xe; cover gas flow purging can increase the proportion of Kr and decrease the proportion of Xe. When the cover gas flow continues purging, the proportions of Kr and I both decrease as the cover gas flow rate increases, while the proportion of Xe decreases in an opposite trend. This is because the radioactivity concentration is connected to the decay constant of radionuclides. Long-lived radionuclides can be more easily purged by gas flow, and short-lived radionuclides can be more easily stored in the cover gas. For Xe, the ^{135}Xe and $^{135\text{m}}\text{Xe}$ isotopes both are short-lived radionuclides; thus, their concentrations would more slowly decrease with a flow rate increase than other Xe isotopes. This leads to the proportion of Xe increasing as the cover gas flow rate increases.

Figure 3b shows that the proportions of various nuclides in the release source terms are somewhat different from the proportions of the nuclide inventories in the cover gas. The basic trend of the lines in the two images is largely the same. The Kr and Xe proportion lines have inflection points at 10 L/min, the probable reason being that radioactive decay is considered in the source calculation.

Figure 4a shows the effect of the cover gas flow rate on the contribution proportions of different types of radionuclides. Comparing Fig. 3b to Fig. 4a, the variation

tendency of the dose contribution proportions of the radionuclides mostly accords with the trend of the nuclide proportions in the source terms except krypton. The variation trend of the dose contribution proportions of the krypton is opposite to that of its proportions in the source terms. This is because of all the isotopes of krypton ^{87}Kr and ^{88}Kr are the most common and their dose conversion factors are several orders of magnitude higher than those of the other isotopes. Their contributions to the effective dose rank in the first position and the third position, respectively. Thus, the range of the dose contribution growth of krypton is greater than the reduction in the range of the proportion in the source term, and the contribution of krypton to the effective dose would increase as cover gas flow rate increases.

Figure 4 also shows the effect of the cover gas flow rate on the contribution proportions of exposure paths in image (b). With the increase in flow rate, the contribution of plume immersion irradiation increases from approximately 71–79% and the proportion of inhalation radiation gradually decreases from approximately 29–21%.

The influence of the cover gas flow rate on 24-h total effective dose is shown in Fig. 5. Obviously, the higher the gas flow rate, the smaller the total effective dose. The trend line smoothly slopes during the final stage showing that the influence of the cover gas leak accident on the maximum

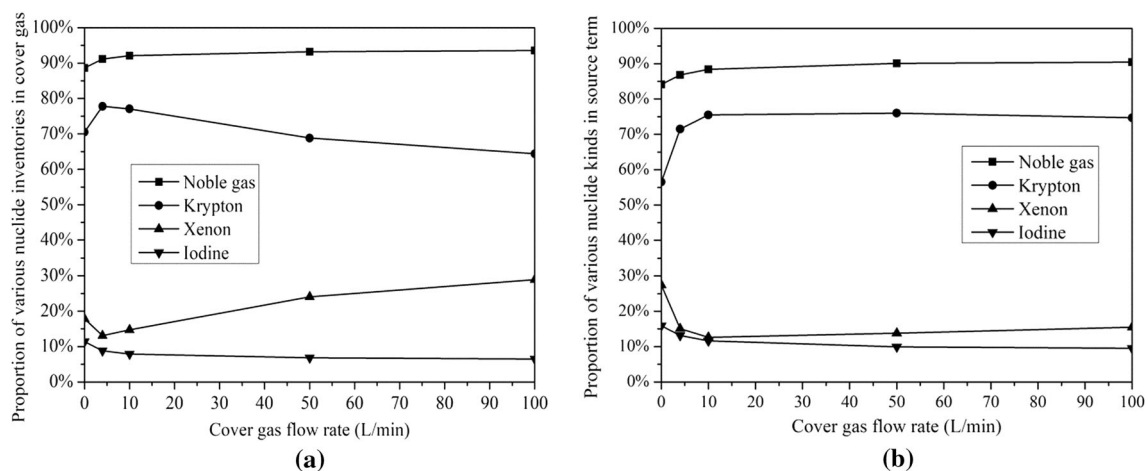


Fig. 3 Influence of cover gas flow rate: **a** Proportions of nuclide inventories in the cover gas; **b** Proportions of various nuclides in the release source terms

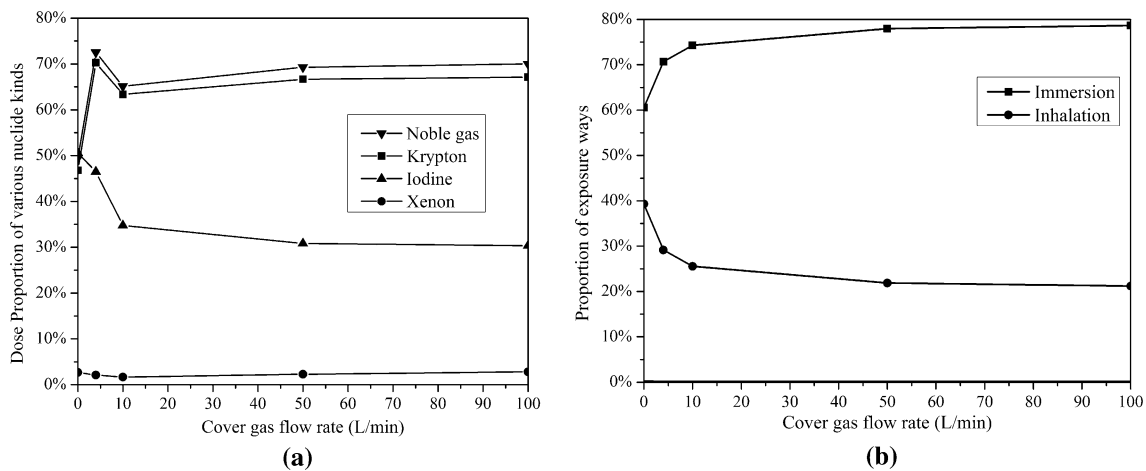


Fig. 4 Contribution proportions of 24-h total effective dose: **a** proportions of radionuclide various types; **b** proportions of exposure paths

credible accident is increasingly less. This is because the radionuclide inventory in the cover gas would decrease as the cover gas flow rate increases.

The point of inflection on this curve appears at approximately 10 L/min, and above 100 L/min the curve is straight which means the influence of the cover gas flow rate is slight. When the cover gas flow rate is changing from 0–10 L/min, the rate has a significant effect on the 24-h total effective dose of the maximum credible accident. The cover gas flow rate also affects the 24-h total effective dose from 50–100 L/min.

5.2 Influence of radioactivity produced during the scram process

In the source term calculation of the maximum credible accident, radioactive products originating from the scrambling process (30 s) were considered. Therefore, these radionuclides affect the dose calculation. The 24-h total

effective dose of the source terms generated during the 30-s scram process is provided in Table 10.

Comparing Table 10 to 8, some dose contributions of the source terms produced by scrambling at the nearest site boundary are provided in Table 11.

As can be seen from Tables 10 and 11, the numerical value of the doses caused by scrambling, whose order of magnitude is no greater than 10^{-2} mSv, is extremely small under the power level of the TMSR-LF1. However, the source terms produced during the scrambling process contribute more than 1% of the 24-h total effective dose of the maximum credible accident. In the case the scram is a failure and manual shutdown is needed, the shutdown time will increase and its dose contribution will also increase.

Dose contributions of source terms produced during the scrambling process are also related to the cover gas flow rate. The higher the flow rate, the greater the dose contribution. This means scram duration would have a greater impact on the consequences of the maximum credible accident as flow rate increases. Therefore, an excessive cover gas flow rate is not necessary because it may reduce the reliability of the safety system.

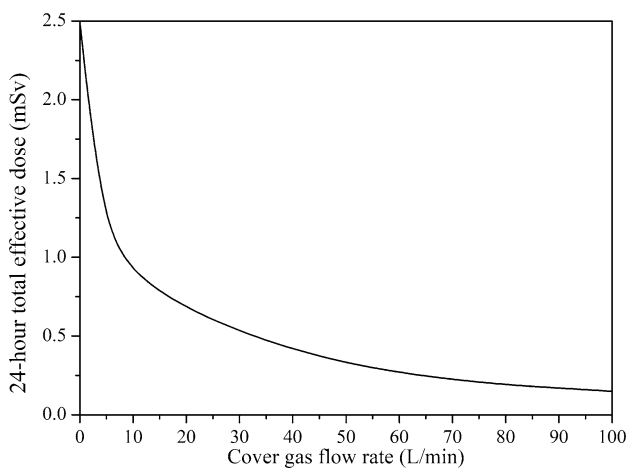


Fig. 5 Influence of cover gas flow rate at 73 m

Table 10 Doses during the scram process

Distance (m)	Dose (mSv)	Distance (m)	Dose (mSv)
50	7.28×10^{-2}	250	3.47×10^{-3}
73	3.37×10^{-2}	300	1.64×10^{-3}
100	1.95×10^{-2}	400	9.77×10^{-4}
150	1.27×10^{-2}	500	6.60×10^{-4}
200	6.25×10^{-3}	1000	4.87×10^{-4}

Table 11 Dose contributions of source terms produced during the scram process at each cover gas flow rate

Flow rate (L/min)	Contribution (%)	Flow rate (L/min)	Contribution (%)
0	1.35	50	13.5
4	2.65	100	22.6
10	4.32		

5.3 Guidance for emergency preparedness

After dose analysis of the maximum credible accident, an emergency class designation of the accident could be the next step. Emergency class is among a minimum set of names or titles for grouping abnormal nuclear reactor conditions according to their relative radiological seriousness; onsite and offsite radiological emergency preparedness actions are necessary to respond to such conditions [27]. The existing radiological emergency classes, in descending order of seriousness, are the emergency classes and corresponding emergency action levels in the Chinese national guidance as shown in Table 12 [25].

Emergency classes for the maximum credible accident under different cover gas flow rate are shown in Fig. 6.

In Fig. 6, at the same location, the emergency class will be lower if the cover gas flow rate is higher. When the cover gas flow rate is greater than 50 L/min, only an abnormal notification would be needed. When the cover gas flow rate is 4–10 L/min, an alert would be needed. When there is no flow rate, a site-area emergency would be needed.

Therefore, when the cover gas flow rate is no less than 4 L/min, a site-area emergency classification can be abolished outside 50 m from reactor in the emergency plan for the TMSR-LF1. Under the same emergency class, if a closer distance is desired, the cover gas flow rate needs to be increased. For this same reason, if a lower flow rate is desired, the distance from the reactor to the building boundary needs to be increased.

6 Conclusion

All the possible accidents of the TMSR-LF1 were analyzed and show that only a cover gas leak would lead to a radiological release to the environment. A cover gas leak was chosen as the maximum credible accident of the TMSR-LF1.

Based on the effective dose calculation of the maximum credible accident, when the cover gas flow rate is 0 L/min, the 24-h total effective dose is 0.04–5.30 mSv. When the cover gas flow rate is 4 L/min, the 24-h total effective dose is 0.02–2.49 mSv. When cover gas flow rate is 10 L/min, the 24-h total effective dose is 0.01–1.63 mSv. When the cover gas flow rate is 50 L/min, the 24-h total effective dose is $3.14\text{E}-03$ –0.47 mSv. When the cover gas flow rate is 100 L/min, the 24-h total effective dose is $1.68\text{E}-03$ –0.25 mSv.

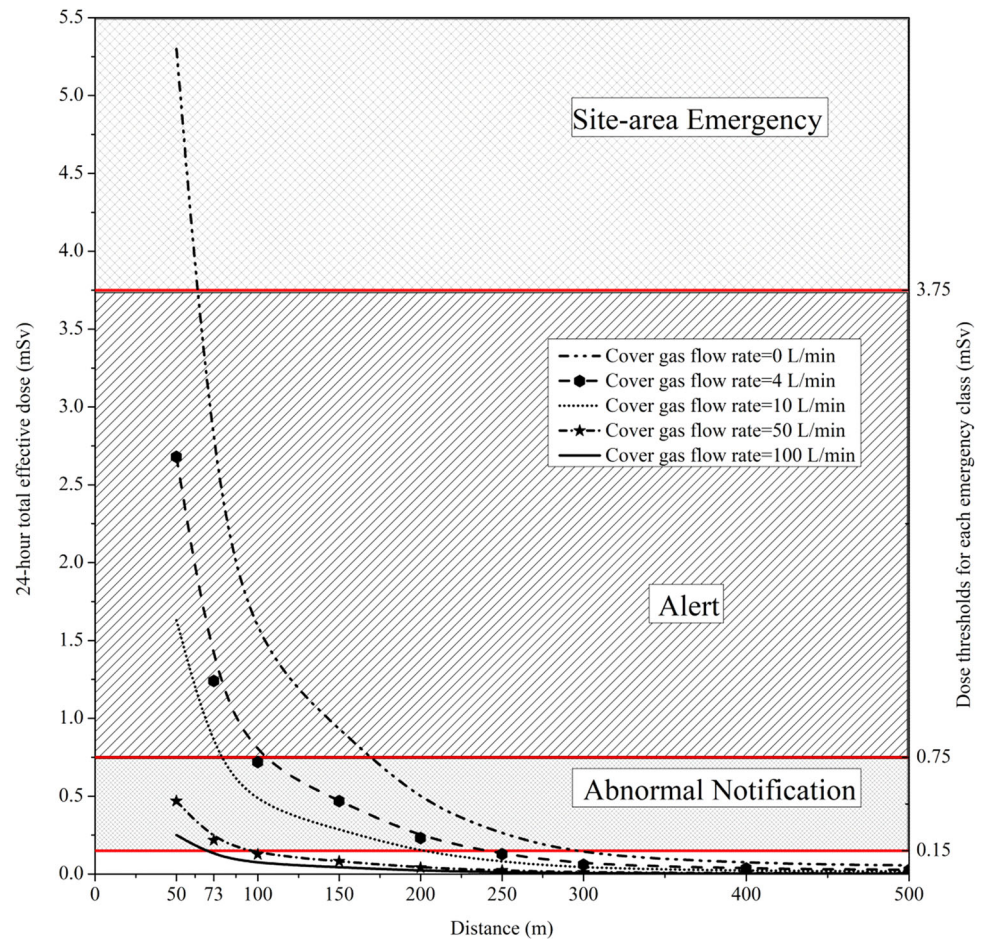
The cover gas flow rate can affect the radiation consequence of the maximum credible accident. When the cover gas flow rate changes from 0 to 10 L/min, the cover gas flow rate has a significant effect on the 24-h total effective dose of the maximum credible accident. The cover gas flow rates are also related to the dose contributions of the source terms produced during the scrambling process. When the flow rate is 10 L/min, the dose contribution of the source terms produced during the scrambling process is approximately 4.32%. Therefore, 10 L/min would be an adaptive cover gas flow rate.

Comparison of the 24-h total effective dose of the maximum credible accident and national guidance for a research reactor emergency, without cover gas flow, indicates that a site-area emergency class would be needed within the 50–73-m range from the reactor. In the case of

Table 12 Emergency action level for a research reactor

Emergency classification	Emergency action level
Abnormal notification	Release of gaseous or liquid radioactivity resulting in a site boundary of a 24-h total effective dose greater than 0.15 mSv
Alert	Release of gaseous or liquid radioactivity resulting in a site boundary of a 24-h total effective dose greater than 0.75 mSv
Site-area emergency	Release of gaseous or liquid radioactivity resulting in a site boundary of a 24-h total effective dose greater than 3.75 mSv
General emergency	Release of gaseous or liquid radioactivity resulting in site boundary of a 24-h total effective dose greater than 10 mSv

Fig. 6 Emergency classes for the maximum credible accident under different cover gas flow rates



cover gas flow, only an abnormal notification and an alert two emergency class would be required more than 50 m from the reactor.

References

- Committee U.S. DOE. A technology roadmap for generation IV nuclear energy systems, GIF-002-00. The generation IV international forum (2002)
- M.H. Jiang, H.J. Xu, Z.M. Dai, Advanced fission energy program-TMSR nuclear energy system. *Bull. Chin. Acad. Sci.* **27**(3), 366–374 (2012). <https://doi.org/10.3969/j.issn.1000-3045.2012.03.016>. (in Chinese)
- D.L. Zhang, L.M. Liu, M.H. Liu et al., Review of conceptual design and fundamental research of molten salt reactors in China. *Int. J. Energy Res.* **42**(5), 1834–1848 (2018). <https://doi.org/10.1002/er.3979>
- Z.H. Zhang, X.B. Xia, J. Cai et al., Simulation of radiation dose distribution and thermal analysis for the bulk shielding of an optimized molten salt reactor. *Nucl. Sci. Tech.* **26**, 040603 (2015). <https://doi.org/10.13538/j.1001-8042/nst.26.040603>
- R.M. Ji, M.H. Li, Y. Zou et al., Impact of photoneutrons on reactivity measurements for TMSR-SF1. *Nucl. Sci. Tech.* **28**, 76 (2017). <https://doi.org/10.1007/s41365-017-0234-7>
- T.J. Dolan (ed.), *Molten Salt Reactors and Thorium Energy* (Woodhead Publishing, Duxford, 2017)
- B.M. Elsheikh, Safety assessment of molten salt reactors in comparison with light water reactors. *J. Radiat. Res. AS.* **6**(2), 63–70 (2013). <https://doi.org/10.1016/j.jrras.2013.10.008>
- C.B. Shi, M.S. Cheng, G.M. Liu et al., Development and application of a system analysis code for liquid fueled molten salt reactors based on RELAP5 code. *Nucl. Eng. Des.* **305**, 378–388 (2016). <https://doi.org/10.1016/j.nucengdes.2016.05.034>
- J. Cai, X.B. Xia, K. Chen et al., Analysis on reactivity initiated transient from control rod failure events of a molten salt reactor. *Nucl. Sci. Tech.* **25**, 030602 (2014). <https://doi.org/10.13538/j.1001-8042/nst.25.030602>
- R.P. Guo, C.L. Yang, Variance of atmosphere dispersion factor for accident release from nuclear power plant. *Adv. Mater. Res.* **518–523**, 1242–1246 (2012). <https://doi.org/10.4028/www.scientific.net/AMR.518-523.1242>
- A. Jones, K. Jones, S. Holmes et al., Assessing the possible radiological impact of routine radiological discharges from proposed nuclear power stations in England and Wales. *J. Radiol. Prot.* **33**, 163–174 (2013). <https://doi.org/10.1088/0952-4746/33/1/163>
- J. Cao, M. Yeung, S. Wong et al., Adaptation of COSYMA and assessment of accident consequences for Daya Bay nuclear power plant in China. *J. Environ. Radioact.* **48**(3), 265–277 (2000). [https://doi.org/10.1016/S0265-931X\(99\)00077-6](https://doi.org/10.1016/S0265-931X(99)00077-6)
- G. Katata, H. Terada, H. Nagai et al., Numerical reconstruction of high dose rate zones because of the Fukushima Dai-ichi Nuclear

- Power Plant accident. *J. Environ. Radioact.* **111**, 2–12 (2012). <https://doi.org/10.1016/j.jenvrad.2011.09.011>
14. S.E. Beall, P.N. Haubenreich, R.B. Lindauer et al., *ORNL-TM-0732, MSRE Design and Operations Report Part V: Reactor Safety Analysis Report* (ORNL, Oak Ridge, 1964)
 15. A. Scale, *Comprehensive Modeling and Simulation Suite for Nuclear Safety Analysis and Design. ORNL/TM-2005/39, Version 6.1* (ORNL, Oak Ridge, 2011)
 16. E.L. Compere, S.S. Kirslis, E.G. Bohlmann et al., *ORNL-4865, Fission Production Behavior in the Molten Salt Reactor Experiment* (ORNL, Oak Ridge, 1975)
 17. G.T. Mays, A.N. Smith, J.R. Engel, *ORNL-TM-5759, Distribution and Behavior of Tritium in the Coolant-Salt Technology Facility* (ORNL, Oak Ridge, 1977)
 18. X.W. Lv, X.B. Xia, Z.H. Zhang et al., Analysis of tritium production in a 2 MW liquid-fueled molten salt experiment reactor and its environmental impact. *Nucl. Sci. Tech.* **27**, 78 (2016). <https://doi.org/10.1007/s41365-016-0100-z>
 19. H. Qin, C.L. Wang, S.Z. Qiu et al., Study of tritium transport characteristics in a transportable fluoride-salt-cooled high-temperature reactor. *Int. J. Energy Res.* **42**, 1536–1550 (2018). <https://doi.org/10.1002/er.3944>
 20. Y.S. Zeng, W.G. Liu, W. Liu et al., Tritium transport analysis in a 2-MW liquid-fueled molten salt experimental reactor with the code TMSR-TTAC. *Nucl. Technol.* (2018). <https://doi.org/10.1080/00295450.2018.1507200>
 21. Y.S. Zeng, W.G. Liu, W. Liu et al., Development of the tritium transport analysis code for the thorium-based molten salt reactor. *Nucl. Technol.* **203**(1), 48–57 (2018). <https://doi.org/10.1080/00295450.2018.1433408>
 22. Yoshioka R, Mitachi K, Shimazu Y, et al., Safety criteria and guidelines for MSR accident analysis, in *PHYSOR 2014-The Role of Reactor Physics Toward a Sustainable Future*, The Westin Miyako, Kyoto, Japan, Sept 28–Oct 3, 2014
 23. L.Z. Cao, K. Zhuang, Y.Q. Zheng et al., Transient analysis for liquid-fuel molten salt reactor based on MOREL2.0 code. *Int. J. Energy Res.* **42**(1), 261–275 (2017). <https://doi.org/10.1002/er.3828>
 24. Shanghai Institute of Applied Physics, Chinese Academy of Sciences, The Site Selection Report of TMSR-LF1. (PRC MEE, 2018), http://www.mee.gov.cn/hyfs_12801/hyfs_lj_sxm_hjyxpj/gs/201802/t20180209_431193.shtml. Accessed 7 Mar 2019. (in Chinese)
 25. NNSA. HAD 002/06, Emergency plan and preparedness for research reactor. (NNSA, Beijing, 1991) (in Chinese)
 26. SAMR and SAC. GB/T 17982, Models and parameters for calculating radiation doses to the public in the emergency of a nuclear accident. (SAMR and SAC, Beijing, 2018) (in Chinese)
 27. AQSIQ. GB 18871, Basic standards for protection against ionizing radiation and the safety of radiation sources. (AQSIQ, Beijing, 2002) (in Chinese)
 28. International Atomic Energy Agency, Safety reports series no. 19, *Generic Models for Use in Assessing the Impact of Discharges of Radioactive Substances to the Environment* (IAEA, Vienna, 2001)
 29. Nuclear Regulatory Commission, Federal guidance report No. 12, *External Exposure to Radionuclides in Air, Water, and Soil*. (NRC, Washington DC, 1993)
 30. Nuclear Regulatory Commission, Regulatory guide 1.195, *Methods and Assumptions for Evaluating Radiological Consequences of Design Basis Incidents at Light-Water Nuclear Power Reactors*. (NRC, Washington DC, 2003)
 31. Nuclear Regulatory Commission, Regulatory Guide 1.194, *Atmospheric Relative Concentrations for Control Room Radiological Habitability Assessments at Nuclear Power Plants*. (NRC, Washington DC, 2003)
 32. J.V. Ramsdell Jr., C.A. Simonen, *NUREG/CR-6331, revision 1, atmospheric relative concentration in building wakes* (NRC, Washington DC, 1997)
 33. A.H. Huber, Wind-tunnel and Gaussian plume modeling of building wake dispersion. *Atmos. Environ. A-Gen.* **25**(7), 1237–1249 (1991). [https://doi.org/10.1016/0960-1686\(91\)90234-X](https://doi.org/10.1016/0960-1686(91)90234-X)